



## Paclitaxel-PHBV nanoparticles and their toxicity to endometrial and primary ovarian cancer cells

Cristian Vilos<sup>a,c</sup>, Francisco A. Morales<sup>a</sup>, Paula A. Solar<sup>a</sup>, Natalia S. Herrera<sup>a</sup>, Fernando D. Gonzalez-Nilo<sup>b</sup>, Daniel A. Aguayo<sup>b</sup>, Hegaly L. Mendoza<sup>b</sup>, Jeffrey Comer<sup>b,h</sup>, Maria L. Bravo<sup>d</sup>, Pamela A. Gonzalez<sup>d</sup>, Sumie Kato<sup>e</sup>, Mauricio A. Cuello<sup>e</sup>, Catalina Alonso<sup>f</sup>, Erasmo J. Bravo<sup>f</sup>, Eva I. Bustamante<sup>g</sup>, Gareth I. Owen<sup>d</sup>, Luis A. Velasquez<sup>a,c,\*</sup>

<sup>a</sup> Universidad Andres Bello, Facultad de Medicina, Center for Integrative Medicine and Innovative Science (CIMIS), Echaurren 183, Santiago, Chile

<sup>b</sup> Universidad Andres Bello, Facultad de Biología, Center for Bioinformatics and Integrative Biology (CBIB), Republica 239, Santiago, Chile

<sup>c</sup> Centro para el Desarrollo de la Nanociencia y Nanotecnología, Universidad de Santiago de Chile, Ecuador 3493, Santiago, Chile

<sup>d</sup> Facultad de Ciencias Biológicas, Pontificia Universidad Católica de Chile, Alameda 340, Santiago, Chile

<sup>e</sup> Facultad de Medicina, Pontificia Universidad Católica de Chile, Alameda 340, Santiago, Chile

<sup>f</sup> Hospital Gustavo Frické, Alvarez 1532, Viña del Mar, Chile

<sup>g</sup> Fundación Arturo López Pérez, Rancagua 878, Santiago, Chile

<sup>h</sup> Fundación Fraunhofer Chile Research, M. Sánchez Fontecilla 310 piso 14, Las Condes, Chile

### ARTICLE INFO

#### Article history:

Received 28 November 2012

Accepted 12 February 2013

Available online 5 March 2013

#### Keywords:

Paclitaxel

PHBV

Nanoparticle

Ovarian cancer

Drug delivery

Molecular dynamics simulations

### ABSTRACT

This report is an integrated study to include the molecular simulation, physicochemical characterization and biological analysis of a paclitaxel-loaded PHBV nanoparticle that demonstrates uptake, release and cytotoxicity in cancer cell lines. Taking this nanoparticle one step closer to its use in a clinical setting, we demonstrate that it causes significant cell death in primary cultures of stage IIIc serous ovarian cancer cells isolated from six patients. Molecular simulations revealed a high affinity of paclitaxel for the water–polymer interface, thus the drug is delivered only when the polymer near it is degraded. The Fourier transform infrared spectroscopy suggests the formation of a short-lived crystalline phase, also observed in the CG simulations, and transmission electron microscopy revealed branched structures on the surface of particles, which disappeared after 4 days. Biological analyses indicated that these particles have a 48-h window of toxicity protection, allowing for the endocytosis of the particle by the cells; this finding was corroborated by confocal microscopy and flow cytometry. The low cost to synthesize PHBV using microorganisms and the potential chemical modifications of the polymer make it attractive for inexpensive, large-scale pharmaceutical production.

© 2013 Elsevier Ltd. All rights reserved.

### 1. Introduction

The worldwide cancer burden continues to grow and is becoming a major economic expenditure for all developed countries. Although the 5-year survival for ovarian cancer patients has improved to nearly 30%, this disease remains the fifth deadliest cancer among American women and is the leading cause of death from gynecologic malignancy. In 2010, 21,880 new cases and 13,850 new deaths were recorded in the United States [1,2].

The major obstacles in the field of oncology include the tremendous effort that is required for early detection, the development of many new drugs and drug delivery systems and the existence of effective chemotherapeutic agents [3,4]. One additional challenge is the development of nanoparticles that meet the clinical demands of therapeutic agents, such as biocompatibility, biodegradability, a clinically relevant circulating half-life, a low rate of intravascular aggregation, and a long-term storage capacity [5]. During the last decade, drug delivery systems based on polymeric nanoparticles have been central to many significant advances in nanomedicine [6]. Accordingly, these particles have generated interest related to their potential use in preclinical and clinical cancer drug development [5].

Polymeric nanoparticles have numerous uses in drug delivery, including the specific and targeted delivery of therapeutic agents,

\* Corresponding author. Center for Integrative Medicine and Innovative Science (CIMIS), Universidad Andres Bello, Facultad de Medicina, Echaurren 183, 8370071, Santiago, Chile.

E-mail address: [luis.velasquez@unab.cl](mailto:luis.velasquez@unab.cl) (L.A. Velasquez).

such as cisplatin [7] and siRNA [8]. In addition, the use of nano-carriers that can cross the epithelial, endothelial or hema-toencephalic barriers [9], the co-liberation of drugs and/or contrast agents that improve the effectiveness of treatments and diagnostic imaging [10], and the encapsulation of highly toxic and poorly water-soluble chemotherapeutics, such as cisplatin, carboplatin and doxorubicin [11], are important. Paclitaxel is a new commercial Taxol preparation; it was originally isolated from the bark of the pacific yew tree (*Taxus Brevifolia*) in 1967. It is the chemotherapeutic agent of choice for the first-line treatment of all stages of ovarian cancer, and it is commonly used to treat endometrial cancer [12].

An advantage of nanoparticles is that they exploit the enhanced permeation and retention (EPR) of the vascular and lymphatic drainage that occurs during the neoplastic process. Thus, by extravasation, these particles deliver the total amount of the encapsulated drug to the tumor cell [13]. Tumors are known to create leaky blood vasculature, permitting the passage of molecules in the nanometer range. Therefore, the design of a biodegradable polymer-based nanoparticle represents an attractive drug delivery option for chemotherapeutics, especially if the drug remains encapsulated and, thus, inactive within the nanoparticle while in the circulation and is preferentially released and activated once inside the tumor cells [13].

Poly(hydroxybutyric-co-hydroxyvaleric acid) (PHBV) is a biodegradable, non-toxic polyester with a low production cost [14]; PHBV has been intensively investigated as a biomaterial for tissue engineering [15] and a microparticle-based drug delivery system [16–18].

Many nanoparticles have been designed for chemotherapeutic drug encapsulation; however, reports on these preparations usually only include their chemical and structural characterization and their activity in a cancer cell line. In this work, based on the suitable properties of PHBV and the broad use of paclitaxel to treat many malignancies, we formulated paclitaxel-loaded PHBV nanoparticles that protect the anticancer agent against premature degradation, provide 48 h of toxicity protection and allow the EPR effect. In addition, we used molecular dynamics simulations to understand the interactions that occur between the polymer and the drug and to elucidate the phenomena that occur during the release process, which is essential to further refine the nanoparticle structure and function to increase the site-specific delivery of the chemotherapeutic cargo. Furthermore, we demonstrate cytotoxicity toward cancer cells lines, and we performed activity assays directly on cancer cells extracted from patients.

## 2. Materials and methods

Poly(3-hydroxybutyric acid-co-hydroxyvaleric acid) (PHBV) with 12 wt. % PVA and polyvinyl alcohol (PVA) (average mol wt. 30,000–70,000) were obtained from Sigma–Aldrich (St. Louis, MO, USA). Nile Red 552/636 was purchased from Invitrogen (Carlsbad, CA, USA). Paclitaxel  $\geq 97\%$  was obtained from Sigma–Aldrich (St. Louis, MO, USA). Dichloromethane (DCM), dimethyl sulfoxide (DMSO) and methanol were purchased from Merck (Darmstadt, Germany).

### 2.1. Preparation and characterization of paclitaxel-encapsulated PHBV nanoparticles (NP-Taxel)

The paclitaxel-encapsulated PHBV nanoparticles (NP-Taxel) were formulated via a modification of the double emulsion ( $w_1/o_1/w_2$ ) solvent-evaporation method [19]. Briefly, 400  $\mu$ L of an aqueous solution containing either 6.84 or 34.2  $\mu$ g/mL paclitaxel (equivalent to treatments used in cell culture experiments; 1 and 5  $\mu$ M, respectively) were added to 1 mL of 3 mg/mL PHBV dissolved in dichloromethane. The first emulsion ( $w_1/o_1$ ) was prepared by sonication in an ultrasonic processor equipped with a microtip probe for 60 s at 125 W in an ice bath. The water-in-oil emulsion was further emulsified by sonication under the same conditions in 4 mL of an aqueous solution of 5 mg/mL PVA ( $w_2$ ). This  $w_1/o_1/w_2$  emulsion was immediately poured into a beaker containing 20 mL of a 0.5 mg/mL PVA solution. The mixture was stirred with an overhead propeller for 12 h under a flow hood, and the solvent was allowed to evaporate. The remaining organic solvent and free molecules were removed by passing the particle solution 3 times through an Amicon Ultra-4 centrifugal filter

(Millipore, Billerica, MA) with a molecular weight cutoff of 100 kDa. NP-Taxel was concentrated by centrifugation and resuspended for use in 500  $\mu$ L phosphate buffered saline (PBS).

The size (diameter, nm) and surface charge (zeta potential, mV) of NP-Taxel was determined by quasi-elastic laser light scattering with a Zetasizer 3000 (Malvern Instruments, UK). Each preparation was suspended in 1 mL phosphate buffered saline (PBS; pH 7.4), and the size and zeta potential were calculated from 11 to 9 independent batches, respectively.

### 2.2. Low-voltage electron microscopy (LVEM)

The NP-Taxel structure was also characterized by low-voltage electron microscopy (LVEM). One drop of the NP-Taxel sample was placed onto an ultra-thin Lacey carbon-coated 400-mesh copper grid and allowed to dry in ambient conditions for 10 min prior to image acquisition, ensuring no more than 1 min of electron beam exposure to the sample. The TEM images were acquired using an LVEM5 electron microscope (Delong Instrument, Montreal, Quebec, Canada) at a nominal operating voltage of 5 kV. The small volume of the vacuum chamber in the LVEM5 microscope facilitates rapid sample visualization within 3 min prior to observation. The low voltage used delivers high contrast in soft materials (up to 20-fold) compared with high-voltage electron microscopes, which use accelerating voltages of approximately 100 kV; this procedure facilitates the omission of staining procedures and allows the direct visualization of biological samples. Digital images were captured using a Retiga 4000R camera (QImaging, Inc., USA) at its maximal resolution.

### 2.3. Paclitaxel encapsulation efficiency and release kinetics

The paclitaxel entrapment efficiency was analyzed using an extraction method described previously by Mao et al. [20]. NP-Taxel (10 mg) was dissolved in 1 mL DCM, followed by the addition of 5 mL methanol and agitation on an orbital shaker at 100 rpm for 24 h at 37 °C. The paclitaxel concentration was determined by ultra-performance liquid chromatography (UPLC) using a standard curve. To measure paclitaxel release, 7 mg NP-Taxel underwent rapid equilibrium dialysis (Thermo Scientific, see manufacturer's instructions) through sequential bag dialysis at 37 °C with gentle shaking in 7 mL of either water or PBS (pH 7.4). At each sampling time, 1 mL of the supernatant was removed and replaced with an equivalent volume of water or PBS. The supernatants were analyzed by UPLC to determine paclitaxel release.

### 2.4. Ultra-performance liquid chromatography (UPLC)

UPLC was performed using an Acquity system (Waters, Milford, MA, USA) equipped with a binary solvent delivery pump, an autosampler and a tunable UV detector. Chromatographic separation was performed using a Waters Acquity BEH C18 column (50  $\times$  2.1 mm, 1.7  $\mu$ m). The mobile phase was a 70:30 (v:v) mixture of methanol and water at a flow rate of 0.4 mL/min. Detection was performed at a wavelength of 290 nm using a 10  $\mu$ L injection volume; the mobile phase of water and methanol was maintained at 27 °C. The internal chromatographic standard solutions (1, 5, 10, 50 and 100 ng/mL) were freshly prepared in a volumetric flask along with the mobile phase [21].

### 2.5. FTIR spectroscopy

We analyzed the spectroscopic profile of NP-Taxel over 5 days during which the samples were suspended in PBS at 25 °C with light agitation. The samples were collected at 0, 1, 2, 3, 4 and 5 days and subsequently lyophilized. In addition, empty-PHBV nanoparticles and the commercial crystal of PHBV were used as controls. The lyophilized samples were mixed with KBr in a 1:2 ratio and were prepared as pellets of 1 cm in diameter. The pills were analyzed using Bruker Vector 22 FTIR Spectrometer (Hardtstrabe, Karlsruhe, Germany), and the data set was analyzed using OPUS software (Optical User Software, Hardtstrabe, Karlsruhe, Germany) and Origin software (6.0, Massachusetts, USA).

### 2.6. All-atom molecular dynamics methods

All-atom models of PHBV and paclitaxel were parameterized in the framework of the CHARMM General Force Field [22] using the ParamChem interface [<https://www.paramchem.org>]. The hydroxyvaleric component of the PHBV was neglected in the all-atom models because it comprised only about 10% of the PHBV by number of monomers and because neglecting it accelerated convergence of the free energy calculation. Thus, we refer to the polymer molecules as PHB. The primary goal of these simulations was to determine the spatial distribution of the paclitaxel, especially whether the paclitaxel would be found predominantly within the polymer layer, within the aqueous phase, or at the interface of the two layers. This distribution should not be overly sensitive to the atomic details of the paclitaxel. Due to the limitations of ParamChem, an additional carbon atom (along with two hydrogen atoms) was added to change the four-member ring of paclitaxel to a five-member ring. We did not expect that this change or the approximate nature of the CHARMM General Force Field would prevent us from roughly determining the

spatial distribution of paclitaxel in the polymer layer. Moreover, the ring in question did not appear to be particularly important for the polymer–paclitaxel interaction. For example, much stronger associations were observed between the phenyl groups of the paclitaxel and the methyl group of 3-hydroxybutyric acid and between the hydroxyl groups of the paclitaxel and the ester of the 3-hydroxybutyric acid.

The all-atom MD simulations described in this paper were performed with the program NAMD 2.9 [23] following established protocols [24].

Briefly, the simulations were performed using a 2-fs timestep, rigid TIP3P water molecules, rigid bonds to hydrogen, a smooth 0.7–0.8-nm cutoff for the van der Waals interactions, and the particle-mesh Ewald method for electrostatics (grid spacing ~0.13 nm). A Langevin thermostat with a damping constant of  $0.2 \text{ ps}^{-1}$  was used to maintain the temperature at 310 K, while a Langevin piston maintained the pressure at 1 atm.

The all-atom simulations were more computationally expensive for a given simulated system size when compared with the coarse-grained simulations described in the next section. Therefore, the all-atom system consisted of only a small patch of the polymer layer, for which the interaction with paclitaxel could be studied. Larger scale features of the polymer nanoparticle were studied in coarse-grained simulations. The all-atom system was constructed in a  $6.3 \text{ nm} \times 6.3 \text{ nm} \times 12.1 \text{ nm}$  periodic box. The molecular weight distribution of the polymer that was used in the experiments was not well characterized; however, the mean length of the polymers at the beginning of the experiments was likely larger than could be feasibly simulated due to the size and time scale constraints on the simulated systems. Therefore, we chose molecules that were 40 monomers in length; these molecules had a radius of gyration of approximately 2 nm in free solution and could be arranged within the systems described here. Although we found that 10-mer PHB molecules were soluble and would not form a stable polymer layer, the polymer layer constructed from the 40-mer PHB molecules remained stable for approximately 180 ns of the all-atom simulation. Thirty pre-equilibrated PHB molecules, consisting of 40 monomers each, were randomly arranged in the region ( $-2 \text{ nm} < z < 2 \text{ nm}$ ). The remainder of the system was filled with water molecules. Ions were added to produce a 150 mM NaCl solution. A single molecule of paclitaxel was placed in the aqueous phase. After energy minimization, the system underwent 180 ns of equilibrium simulation to allow for the relaxation of the PHB layer and to ensure that this layer appeared stable. Subsequently, the potential of mean force (PMF), as a function of the distance along the  $z$  axis between the center of mass of the paclitaxel and the center of mass of the PHB layer, was determined by the adaptive biasing force method (ABF) [25,26]. Ten ABF simulations were performed to sample different ranges of this distance for a total simulation time of 477 ns.

### 2.7. Coarse-grain molecular dynamics methods

Coarse-grain molecular dynamics simulations were performed using a model of PHBV developed within the MARTINI framework [27]. The MARTINI framework used for the coarse-grained simulations is sufficiently coarse that similar, but chemically distinct, species may have the same parameterization. For example, dodecane conventionally is parameterized identically to decane. Similarly, our coarse-grained model did not distinguish between hydroxyvaleric and hydroxybutyric monomers. Each PHBV monomer consisted of two beads that were assigned the standard MARTINI types, SNa and SC5, as these parameters gave the best agreement with the water content of the polymer layer seen in the all-atom simulations. Bond and angle parameters were calibrated to correspond to the all-atom simulations.

The coarse-grained simulations were performed with Gromacs 4.5.5 [28] using a 30 fs timestep. The temperature was maintained at 310 K by the velocity-rescaling thermostat [29] and the pressure was maintained at 1 atm using a Berendsen barostat. The system was constructed in a  $38 \text{ nm} \times 38 \text{ nm} \times 38 \text{ nm}$  periodic box. 1222 PHB molecules consisting of 40 monomers each were randomly placed in a spherical shell around the center of the system at a radius  $60 < R < 150$ . Following energy minimization, dynamics were performed under equilibrium conditions for 60 ns.

### 2.8. Cell lines

The endometrial cancer cell line Ishikawa [30] was altered in the Owen laboratory to stably express the ZsGreen-N1 green fluorescent protein (Clontech, Franklin Lakes, NJ). Briefly, this cell line was stably transfected using Lipofectamine® (Invitrogen, Grand Island, NY) according to the manufacturer's instructions, and clonal cell populations that were resistant to G418 were expanded in culture. The cells were maintained in DMEM/F12 medium (Invitrogen) supplemented with 10% (v/v) fetal bovine serum (FBS, Gibco) and 1% (v/v) penicillin/streptomycin (Gibco) and periodically supplemented with 300  $\mu\text{g}/\text{mL}$  G418 (Calbiochem). The ovarian cancer cell line SKOV3 was also maintained in DMEM/F12 medium (Invitrogen) supplemented with 10% (v/v) fetal bovine serum (FBS, Gibco) and 1% (v/v) penicillin/streptomycin (Gibco) [31].

### 2.9. Ovarian cancer primary culture

Ovarian cancer tissue was obtained with patient consent and ethical committee approval from the Oncology-Gynecology Department of the Hospital of the Pontificia Universidad Católica de Chile, Santiago, Chile and the Hospital Gustavo Frick, Viña del Mar, Chile. Samples were obtained from either cytoreduction operations to

remove the primary tumors or catheter drainage in patients presenting with ascites (liquid in the peritoneal cavity). Each cancer culture represented was derived from stage III papillary serous ovarian carcinomas. The establishment of primary cultures of ovarian cancer cells has been previously described. Briefly, immediately after surgery, approximately 1–2  $\text{cm}^3$  of cancerous tissue was separated under sterile conditions and collected into warm saline serum. The tumor was dissected mechanically in a petri dish in the presence of trypsin (Gibco) for 1 min. The cells were washed in serum-containing medium, centrifuged, resuspended in DMEM/F12 with 10% FBS and incubated at 37°C for 48 h in 5%  $\text{CO}_2$ . Ovarian cells obtained from ascitic fluid were centrifuged, resuspended in the aforementioned medium and plated directly. Primary cultured cells from both preparations were expanded to obtain sufficient cell numbers to allow for analysis by the MTS assay in the presence of paclitaxel or NP-Taxel.

### 2.10. Confocal laser scanning microscopy

To examine the uptake of nanoparticles in Ishikawa cells, Nile Red 552/636 dye was encapsulated into PHBV nanoparticles using the same protocol utilized for paclitaxel. The Ishikawa cells were grown in BD Falcon 8-well CultureSlides and treated with 3  $\mu\text{g}/\text{mL}$  NP-Nile Red for 0–48 h. At the indicated time points, the cells were fixed with methanol and analyzed by confocal microscopy (LSM 510, Carl Zeiss, Germany). Stacking analysis was recorded at each time point using eight cross-sections. Image-J (NIH) was used to quantify the fluorescence intensity of each cross-section, and each experiment was performed in triplicate.

### 2.11. MTS assay and flow cytometry analysis

Cell viability was measured by the MTS assay (Promega) and flow cytometry as previously described [32,33].

## 3. Results and discussion

### 3.1. Preparation of NP-Taxel, loading and encapsulation efficiency

The objective of this paper was to obtain nanoparticles that will protect an anticancer agent against premature degradation and allow the EPR effect without toxic side effects. To meet these demands, we chose to use PHBV over the more widely studied polymer PLGA. PHBV has physicochemical properties similar to PLGA, but due to its biotechnological production using bacterial fermentation, it is now a more cost effective alternative. PHBV has been proven useful in the clinical setting, as it is incorporated as “scaffolding” in tissue engineering and in the construction of microparticles in drug development. We prepared PHBV nanoparticles using a modification of the double emulsion solvent-evaporation method. Briefly, to develop paclitaxel-loaded PHB nanoparticles, an aqueous solution of paclitaxel was emulsified in dichloromethane (DCM)-dissolved PHBV. A second emulsification step was performed by adding polyvinyl alcohol, followed by sonication. The resulting solution was placed on an orbital shaker, and the solvent was allowed to evaporate. Solidified, loaded PHBV particles were harvested, spin filtered and characterized. To evaluate the paclitaxel-loading capacity of the PHBV particles, we performed an extraction method in which an amount (i.e., 3 mg) of particles was dissolved in DCM to free the encapsulated drug, and this solution was evaporated and subsequently resuspended in methanol for quantification by UPLC. Table 1 demonstrates the quantity of loaded paclitaxel, which is represented in  $\mu\text{g}$  of paclitaxel/mg of PHBV particle. As expected, the particles incorporated with higher initial concentrations of paclitaxel possessed higher final loading concentrations of this drug. In fact, the proportion remained the same; the polymer loaded with 5  $\mu\text{M}$  (as opposed to 1  $\mu\text{M}$ ) of drug, resulted in particles containing nearly five times as much paclitaxel. In accordance with this linearity, we observed that particles encapsulated approximately 37% in both conditions.

### 3.2. Characterization of size and charge

By light scattering, the average diameter was estimated in a range of 228–264 nm as shown in Table 1, increased paclitaxel incorporation did not significantly change the hydrodynamic

**Table 1**

Determination of the loading yield, encapsulation efficiency, size and zeta potential from nanoparticles loaded in the presence of 1  $\mu$ M or 5  $\mu$ M paclitaxel (NP-Taxel) and non-loaded nanoparticles (NP-empty).

Preparation	Loading <sup>a</sup>	Encapsulation efficiency (%)	Size (nm)	Zeta potential (mV)
	(n = 4)	(n = 4)	(n = 11)	(n = 9)
NPs – empty	ND	ND	264.4 $\pm$ 70.7	-8.9 $\pm$ 2.7
NP-Taxel 1 $\mu$ M	0.40 $\pm$ 0.09	34.9 $\pm$ 2.0	228.1 $\pm$ 25.1	-7.4 $\pm$ 1.8
NP-Taxel 5 $\mu$ M	2.42 $\pm$ 0.20	39.6 $\pm$ 4.2	261.9 $\pm$ 35.1	-6.0 $\pm$ 1.4

ND, not determined.

<sup>a</sup> Loading yield  $\mu$ g drug/mg NP-Taxel.

diameter of the nanoparticle. This is an optimal size for passive liberation in the future clinical use of this nanoparticle [34]. It has been suggested that a beneficial characteristic of nanoparticles for biomedical use is the presence of a negative charge on the outer coat. This negative charge will theoretically reduce aberrant protein binding and, thus, is less likely to activate the immune system, resulting in a longer circulatory half-life. In addition, a negative charge minimizes non-specific binding with the cell surface [35]. The particle was also evaluated for its zeta potential by light scattering. As also shown in Table 1, the zeta potential ranged from -6 to -8.9 mV, with no significant differences between each preparation.

### 3.3. Segregation of paclitaxel to the polymer–water interface

To better understand the microscopic details of the paclitaxel release process, we performed all-atom molecular dynamics simulations of a system containing a PHB layer, an aqueous phase, and paclitaxel. The behavior of the system was first studied in a 180-ns equilibrium simulation, wherein we observed that the PHB layer was stable on this time scale. We also observed that the polymer layer was water permeable. As shown in the mass density plot in Fig. 1A, the PHB layer contained about 10% water by mass. The single paclitaxel molecule spent a majority of the simulation at the polymer–water interface.

To better characterize the interaction between the paclitaxel and PHB layer, we performed a hydrogen bond (H-bond) analysis on the

equilibrium trajectory. The first 14 ns of the trajectory were discarded to reduce the extent to which the results depended on the starting configuration. Snapshots from the trajectory were extracted at 10 ps intervals; for each snapshot, the H-bonds between the paclitaxel and the polymer were identified when the donor–acceptor distance was <0.35 nm and the donor–H–acceptor angle was greater than 120°. The average number of H-bonds during the 166 ns trajectory was 0.26  $\pm$  0.01. Interactions between the hydroxyl groups of the paclitaxel and the carbonyl of the PHB accounted for 75.0% of the H-bonds, while interactions between the peptide nitrogen of the paclitaxel and the carbonyl of the PHB comprised 22.6% of the H-bonds. The remaining H-bonds involved the PHB terminal hydroxyl groups. The PHB molecules used in the simulations (40 monomers) were likely shorter than those present in the experiments, leading to a higher density of chain-terminating hydroxyls in the simulations than in the experiments. However, only 3% of the H-bonds involved the terminal monomers, and only 2.4% of the H-bonds involved the terminal hydroxyl groups of the polymer. Therefore, similar results would likely have been obtained with longer PHB molecules.

To unequivocally determine the energetics of the interaction between paclitaxel and the PHB layer, we calculated the PMF as a function of the distance between the center of mass of the paclitaxel molecule and the center of mass of the PHB layer along the axis orthogonal to the polymer layer (z axis).

### 3.4. Microscopic structure of PHBV nanoparticles

A complete all-atom MD simulation of a nanoparticle in water would require the simulation of tens of millions of atoms, and therefore, extensive all-atom simulations of nanoparticles are prohibitively expensive. Coarse-grained MD, in which a single particle represents several atoms, makes the simulation of large nanoparticle assemblies [36]. Thus, we constructed a coarse-grained model of our PHBV nanoparticles in order to determine their nanoscale structure. Fig. 1C reveals the structure of a stable, quasi-spherical nanoparticle with a diameter of 24 nm that is composed of 40-monomer PHBV molecules.

The coarse grain simulations show pores on the surface of the sphere, in agreement with previous experimental results [37]. Therefore, if the drug is diluted in the solvent inside of the sphere,

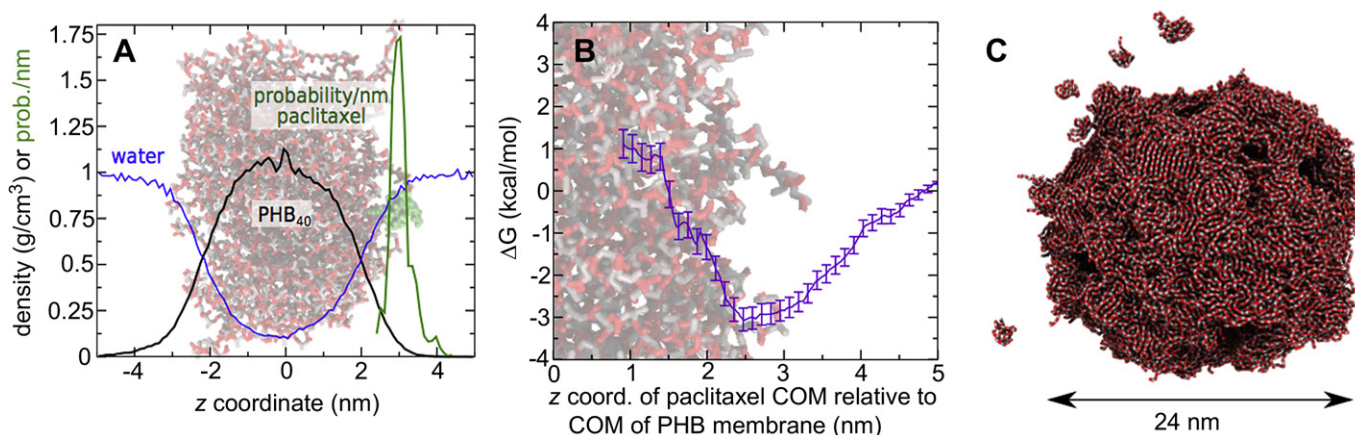


**Fig. 1.** Computer simulations of PHB–paclitaxel interaction and nanoparticle structure. (A) Stable PHB layer in an equilibrium all-atom simulation. The mass densities of the polymer and water components are shown as black and blue lines, respectively. The probability density along the z axis of the single paclitaxel molecule is shown as a green line. A snapshot of the final frame of the simulation is overlaid on the plot. PHB is shown in red and gray, and paclitaxel is shown in green. Water molecules, ions, and hydrogen atoms are not shown. (C) The potential of mean force (PMF) for the interaction between paclitaxel and PHB layer was calculated from an adaptive biasing force simulation. The minimum of the PMF corresponds to the maximum of the paclitaxel probability in the equilibrium simulation (panel B). The thickness of the line represents the standard error of the PMF. (A) Snapshot from the coarse-grained MD simulation of a 24-nm diameter PHBV nanoparticle. The thickness of the shell is about 3 nm, and it contains a number of holes and defects. Water and ion particles are not shown. (For interpretation of the references to colour in this figure legend, the reader is referred to the web version of this article.)

the drug might conceivably diffuse rapidly to the outside of the NP through the pores; however, this does not occur, likely due to strong attraction between the paclitaxel and the polymer surface. Thus, while porous particles are often assumed to accelerate release of the drug, our simulations suggest that porosity could, on the contrary, delay release by providing a larger surface area for paclitaxel binding. The drug might only then be released when nearby polymer is chemically degraded.

### 3.5. TEM characterization using low-voltage electron microscopy and analysis by FTIR spectroscopy

Transmission electron microscopy (TEM) is an excellent method to characterize NPs; however, the high-voltage used in traditional electron microscopy prevents the direct observation of soft-matter structures. In this work, we performed low voltage electron microscopy (LVEM) at 5 kV without metal staining to obtain high contrast images of the nanoparticle structure at different degradation states. An LVEM image of an unstained NP-Taxel droplet is shown in Fig. 2. Notably, the size of the NP-Taxel at day 0 (Fig. 2A) is smaller than at day 5 (Fig. 2F). During the intermediate days (Fig. 2B–D), the NP-Taxel was surrounded by branched structures, presumably consisting of polymer. Interestingly, these structures were no longer present at day 4 (Fig. 2D), leaving an apparent spherical shape with a smooth surface of nanoparticles (Fig. 2D, E). The branched structures likely have a lower density than the polymer layer forming the nanoparticle, which may explain their relatively rapid disappearance.

NP-Taxel exhibited a different fingerprint region than the PHBV crystals because the nanoparticles have a more complex composition, including PHBV-Taxel-PVA. PHBV unmasked the Taxel signal because the interactions predominantly included PHBV. As illustrated in Fig. 3, the spectrum showed carboxyl groups (bands at  $1680\text{--}1725\text{ cm}^{-1}$ ) in the empty PHBV nanoparticles and at day 0 of degradation to NP-Taxel. The aldehyde groups increased between days 1 and 3 of degradation (bands at  $2820\text{--}2900$  and  $2775\text{--}2700\text{ cm}^{-1}$ , and  $1660\text{--}$

$1740\text{ cm}^{-1}$ ), and on the same days, we also observed an increase in the alcohols groups (bands at  $3550\text{--}3200\text{ cm}^{-1}$ ), the signal to crystallization in the polymer and in broken-in ester groups. This fact is very important because if a signal to the ester groups is broken and aldehyde and alcohol groups are formed. This reaction is possible because the degradation occurred at a pH of 7.2; if this reaction occurs at an acidic pH, then cleavage next to the ester bond would occur, and this reaction would form carboxyl groups instead of aldehyde groups. Finally, these results suggest that the polymer experienced localized crystallization for canaliculated formation, through which water could enter and complete the degradation by polymer hydrolysis.

### 3.6. Uptake of Nile Red-loaded PHBV nanoparticles

Before testing the anticancer capacity of the NPs, we sought to confirm the ability of cancer cells to uptake PHBV nanoparticles. To this end, we synthesized PHBV nanoparticles containing the hydrophobic dye Nile Red (see methods). These nanoparticles were washed with water, resuspended in PBS and added to culture medium in 6-well culture dishes containing a growing monolayer of the human endometrial carcinoma cell line Ishikawa, which was stably transfected with green fluorescent protein (ZsGreen, see methods). As shown in Fig. 4A, nanoparticles were observed at 30 min and uptake continued to increase over 48 h. The intracellular incorporation of Nile Red was confirmed by stacking analysis using confocal microscopy, as shown by the representative images in Fig. 4A (thin image), which are quantified in Fig. 4B. More complete confocal microscopy z-stack images are shown in the Supplementary figures.

### 3.7. In vitro release of paclitaxel

As the retention of the chemotherapeutic drug within the nanoparticle is fundamental for its future clinical application, we next measured the liberation of paclitaxel from the PHBV nanoparticle in non-biological conditions. As shown in Fig. 5, paclitaxel-

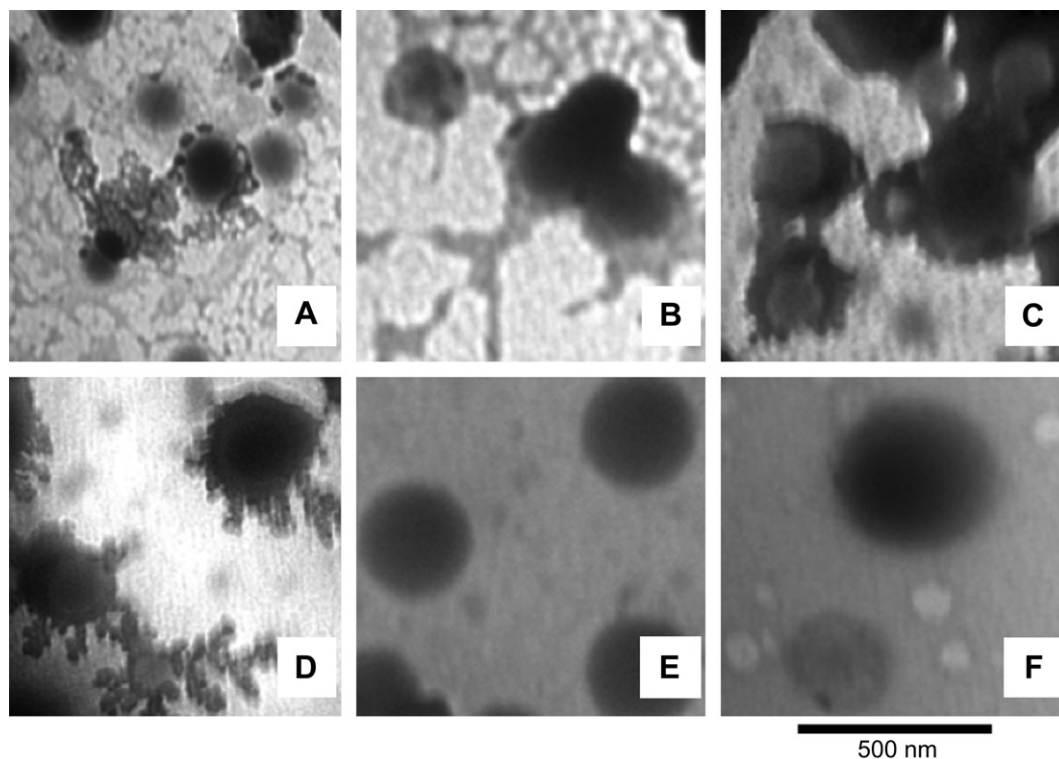


Fig. 2. Time-dependence of the NP-Taxel size and surface-polymer structures during Taxel liberation processes observed using LVEM. 0 (A), 1 (B), 2 (C), 3 (D), 4 (E) and 5 (F) days.

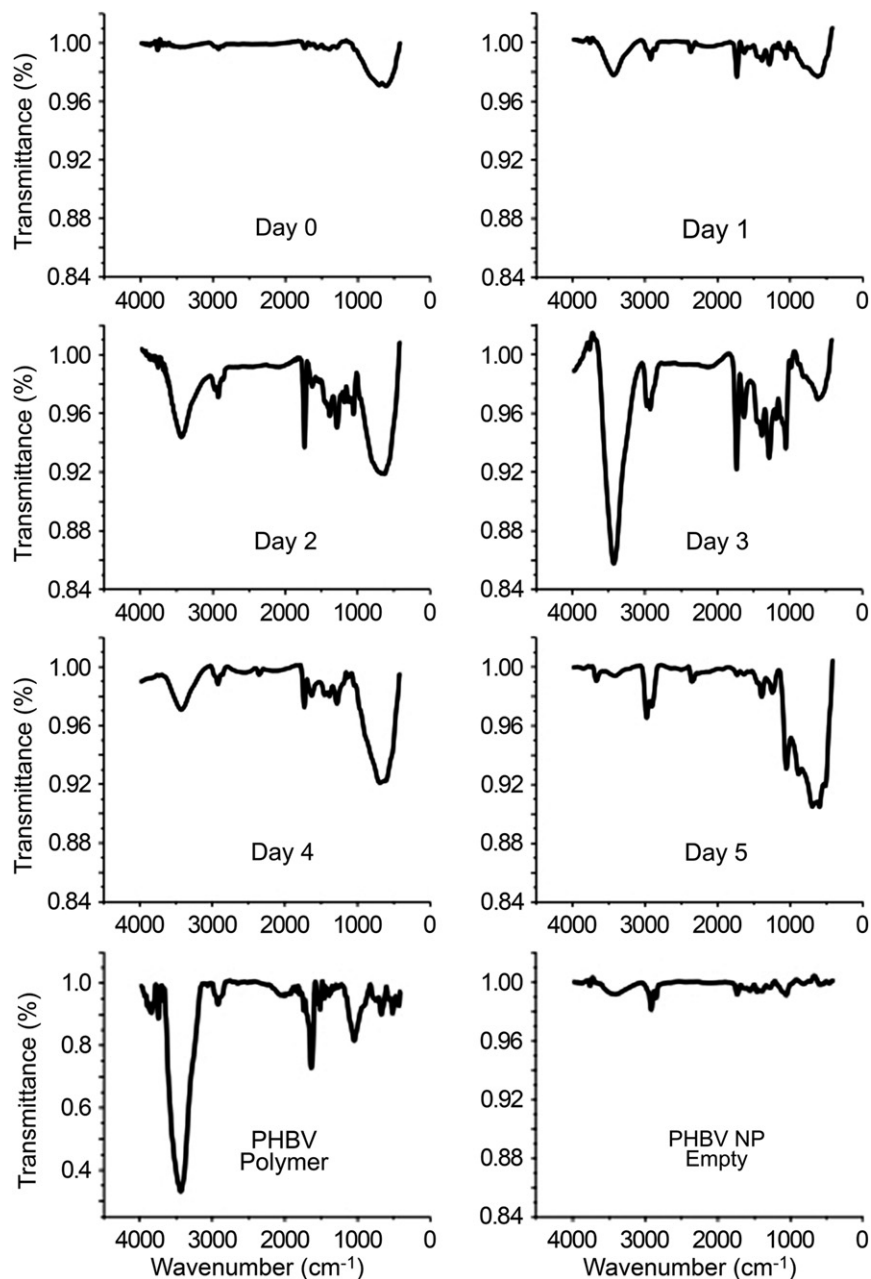


Fig. 3. FTIR spectroscopy of paclitaxel-loaded PHBV nanoparticles from a time course in vitro release system (0–5 days).

containing nanoparticles that were resuspended in distilled water demonstrated less than 4% release over a 5-day period at 25 °C. However, in a more physiologically relevant solution, PBS pH 7.4, less than 1% was liberated over a 5-day period. These results suggest high specificity for any potential future use of this nanoparticle, as less than 1% of paclitaxel would be liberated into the circulation, and given the leaky blood vasculature that irrigates tumors, this nanoparticle should be taken up preferentially by the cancer cells.

### 3.8. Cytotoxicity of NP-Taxel in Ishikawa cells

To evaluate the biological activity of paclitaxel-containing nanoparticles (referred to hereafter as NP-Taxel) we assessed the cytotoxicity using the MTS assay previously shown in our laboratory

to reflect apoptotic cell death in the presence of paclitaxel [32]. Fig. 6 shows that paclitaxel alone is capable of bringing about cell death at 0.1  $\mu\text{M}$ . The three concentrations of paclitaxel used demonstrated the same effect at each time point measured, with the exception of 0.1  $\mu\text{M}$  at 2 days. Interestingly, NP-Taxel in a quantity that delivers 0.1  $\mu\text{M}$  of paclitaxel did not induce cytotoxicity at any time point and had the unexpected effect of increasing proliferation (or at least the redox state of the cells, which is measured in this assay). However, 1  $\mu\text{M}$  NP-Taxel initiated cell death after four days of treatment and 5  $\mu\text{M}$  NP-Taxel induced cell death at times and concentrations undistinguishable from 1 to 5  $\mu\text{M}$  paclitaxel. This result suggests that 5  $\mu\text{M}$  NP-Taxel liberates at least an equivalent of 1  $\mu\text{M}$  paclitaxel. This liberation is more than acceptable for any given future commercial application, as the estimated circulatory concentration of paclitaxel in patients is between 4 and 10  $\mu\text{M}$  and theoretically the

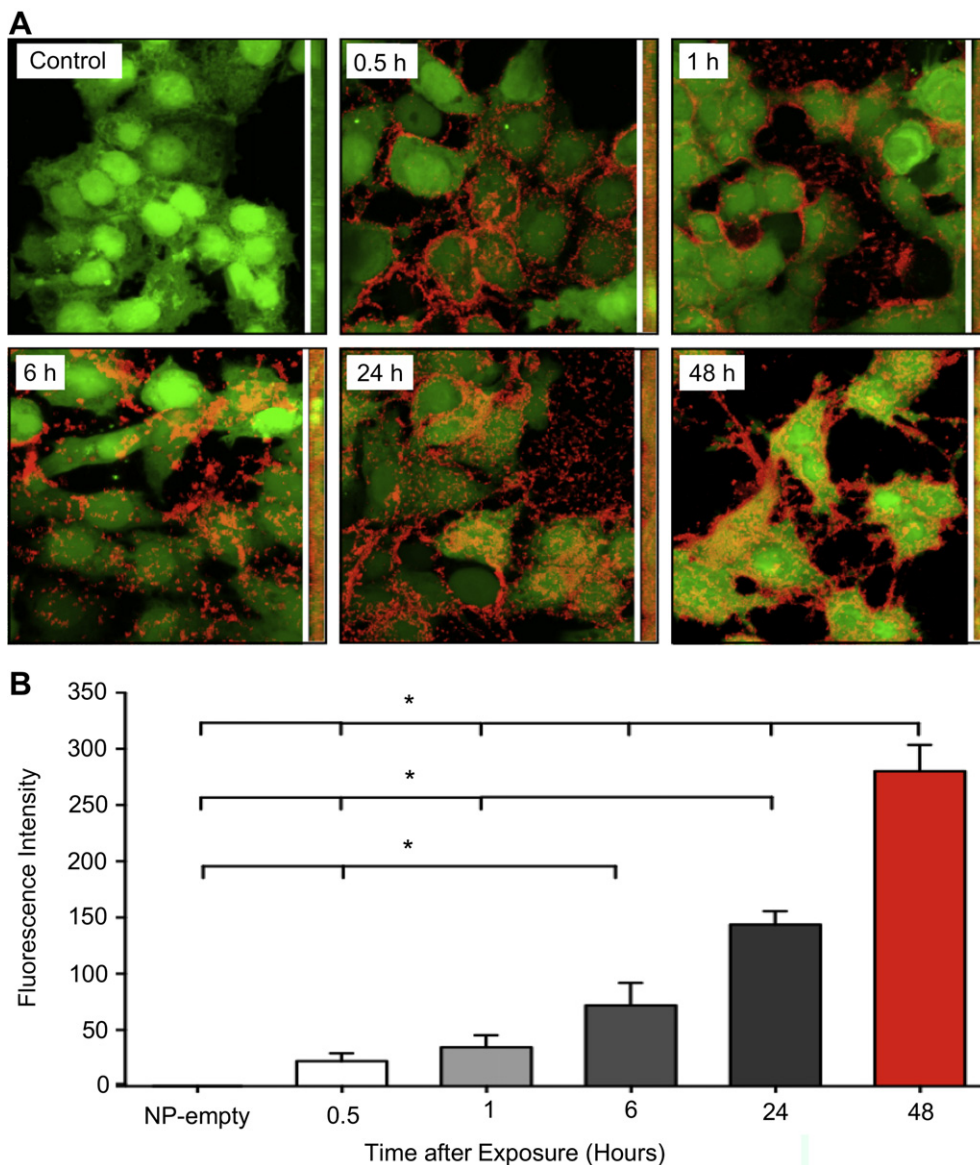


**Fig. 4.** (A) Fluorescence confocal microscopy demonstrating the uptake of Nile Red-loaded PHBV nanoparticles in the Ishikawa cancer cell line, which had been previously stably transfected with green fluorescent protein. The thin image on the side of each principal image demonstrates a stacking analysis by confocal microscopy, confirming the intracellular incorporation of the nanoparticles. (B) Determination of the fluorescence intensity at time points after exposure ( $n = 3$ ),  $^*p < 0.05$  Kruskal–Wallis and Mann–Whitney post-test.

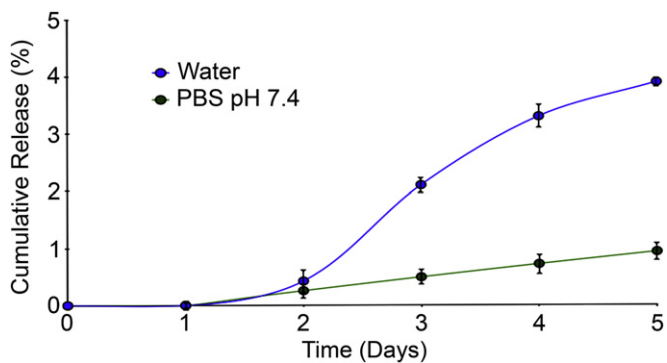


**Fig. 5.** Time course in days demonstrating the cumulative release of paclitaxel from 5  $\mu$ M-loaded nanoparticles in the presence of water (blue line) or PBS, pH 7.4 (green line). (For interpretation of the references to colour in this figure legend, the reader is referred to the web version of this article.)

nanoparticles will be within the cancer cell at the moment of paclitaxel release [38].

### 3.9. Mechanism of cell death

To further understand the effect of NP-Taxel at earlier time points and to confirm whether the NP-Taxel induced cell death occurs through the same mechanisms as reported for paclitaxel, we used flow cytometry to assess changes in the cell cycle at 24 and 48 h and measured cell death by the occurrence of a sub G0/G1 peak in the cell cycle profile. As shown in Fig. 7, empty PHBV nanoparticles (i.e. without paclitaxel) produced the same cell-cycle profile at both 24 and 48 h. In accordance with the literature, paclitaxel alone induced a cell cycle arrest in G2/M before instigating cell death (Fig. 7A, paclitaxel 5  $\mu$ M). Interestingly, the incubation of paclitaxel together with empty PHBV nanoparticles had a protective effect against cell death, with the majority of the cancer cells being in G2/M arrest at 24 h (this protective effect will be

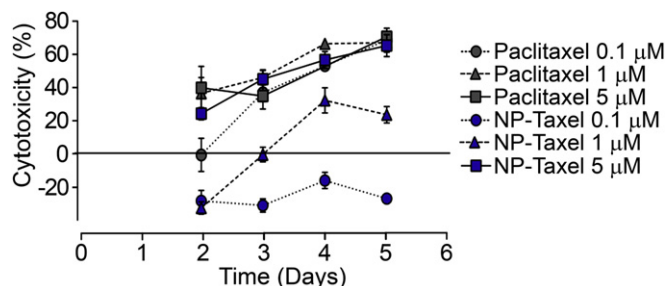


**Fig. 6.** The treatment of Ishikawa cancer cells with 5  $\mu\text{M}$  paclitaxel-loaded nanoparticles generated similar cytotoxicity to that of 1  $\mu\text{M}$  paclitaxel as measured by the MTS assay. The treatments were performed for 48–120 h with different concentrations of NP-Taxel or paclitaxel alone (0.1, 1 and 5  $\mu\text{M}$ ). ANOVA, post-test Bonferroni demonstrated no significant differences between 5  $\mu\text{M}$  NP-Taxel and either 1 or 5  $\mu\text{M}$  paclitaxel alone.

discussed later). The presence of 5  $\mu\text{M}$  NP-Taxel demonstrated G2/M arrest at 24 h but not cell death, mirroring the result of paclitaxel with empty PHBV nanoparticles. At 48 h, NP-Taxel had induced cell death in the majority of the cancer cells analyzed (Fig. 7B). These results demonstrate that paclitaxel-loaded PHBV nanoparticles confers cell death by the same mechanism (first an arrest in G2/M and then apoptosis) as paclitaxel as a single agent.

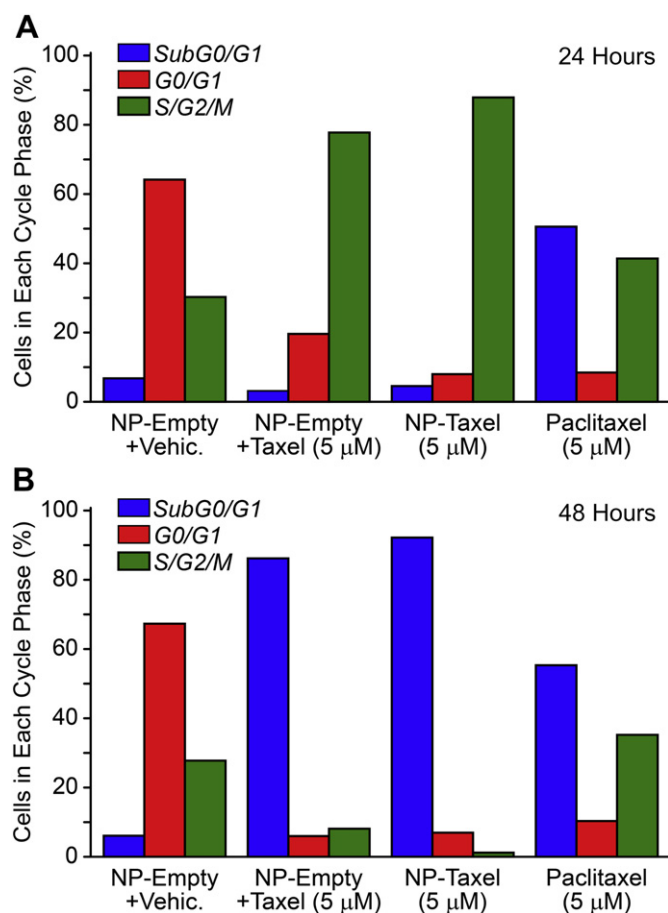


**Fig. 7.** The observation of a preliminary G2/M cell cycle arrest suggests that paclitaxel-loaded nanoparticles induce cell death by the same mechanism as that of paclitaxel alone. The cell cycle analysis was performed by flow cytometry in the Ishikawa cancer cell line after 24 h (A) or 48 h (B) of treatment with NP-Taxel or paclitaxel alone at the stated concentrations. For the graphical representation, the cell cycle was divided into non-proliferative (G0/G1), proliferative (S/G2/M) and cell death (peak sub G0/G1) region.

### 3.10. Cytotoxicity of NP-Taxel in SKOV3 cells

To demonstrate that the effects observed in the endometrial cell line Ishikawa are not exclusive to this cell line or this type of cancer, we assessed the cytotoxicity of NP-Taxel in the human ovarian cancer cell line SKOV3. As demonstrated previously [32], this cell line is sensitive to paclitaxel-induced cell death from 0.1  $\mu\text{M}$  onwards (Fig. 8). However, unlike the endometrial cancer cells, the SKOV3 cell line did not demonstrate a proliferative or a protective effect when empty NPs were administered either alone or in the presence of free paclitaxel. During the window of protection, this result demonstrates that the protective effect of empty nanoparticles is cell specific (this will be discussed in detail below). However, as observed in Ishikawa cells, the addition of NP-Taxel induced cell death equivalent to that of 1  $\mu\text{M}$  paclitaxel.

### 3.11. Cytotoxicity of NP-Taxel in primary cultures of ovarian cancer

To determine the clinical relevance of this assessment of biological activity, we examined the effect of NP-Taxel in primary cultures of ovarian cancer. These cancer cells were obtained from the primary culture of either tumor or ascitis (fluid extracted from the peritoneal cavity) obtained with informed consent from patients undergoing treatment for stage IIIc papillary serous ovarian cancer. As expected for six individual patients, the response to paclitaxel was distinct in each case. The level of cytotoxicity observed with NP-Taxel was lower than that of paclitaxel in each primary culture, but still produced significant cell death in each case analyzed. This result demonstrates that cell death occurred within 48 h of the primary culture of ovarian cancer cells. As previously mentioned, in future clinical applications, this NP-Taxel mediated cell death may be greater than paclitaxel alone due to the incorporation of the nanoparticles and drug release directly in the cancer cells and possibly a prolonged half-life compared to paclitaxel alone, due to the necessity of polymer breakdown in the lysosome to facilitate drug release.

Interestingly, as observed in the human endometrial cancer cell line and in two of six ovarian cancers derived from patients, the empty nanoparticles demonstrated cellular cytotoxicity (Fig. 9 patients 5 & 6), as was observed in the ovarian cancer cell line SKOV3. Furthermore, four primary cultures of ovarian cancer demonstrated proliferation in the presence of empty NP. This result further demonstrates the well-known clinical observation that no two cancers are alike and no two patients respond in exactly the same way to a given therapy. However, the question remains as to why a polymer complex such as PHBV/PVA could bring about cell death or survival. The nature of PHBV (3-hydroxybutyric acid-co-hydroxyvaleric acid) suggests the potential liberation of hydroxybutyric acid in the living cell. Hydroxybutyric acid, which is a ketone body that is produced in vivo in humans, is a group of four-carbon organic compounds that possess both hydroxyl and carboxylic acid functional groups. In cancer cells, this compound may be broken down into derivatives such as D-3-hydroxybutyrate, DL-3-hydroxybutyrate and methyl (D)-3-hydroxybutyrate [39]. In mouse glial cells, DL-3-hydroxybutyrate has been previously shown to possess a protective effect against apoptosis, while D-beta-hydroxybutyrate prevents against neurotoxicity in rat glial cells (PC12) [40]. Furthermore, ketone bodies have been reported to be favorable alternative metabolic substrates and are protective in the face of several pathologies. A rich ketogenic diet has also been shown to reduce cytochrome c release and thus cellular apoptosis in a neurological model [41]. Conversely, the liberation of alcohol groups from PVA (polyvinyl alcohol) could lead to oxidative stress within cancer cells and thus cell death. The metabolic state of the cell and the accompanying stimulus present at any given time may represent the factors that tip the balance of how the cell responds to these nanoparticles. Irrespective of the

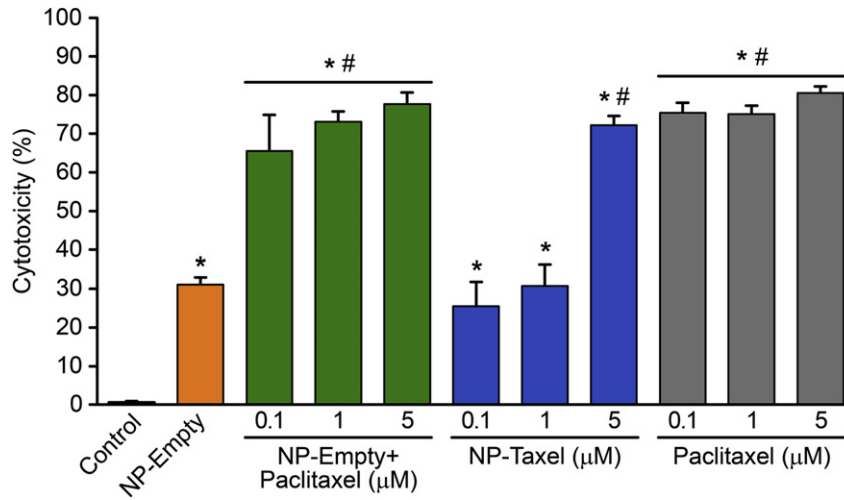


**Fig. 8.** Paclitaxel-loaded nanoparticles induced cell death in the ovarian cancer cell line SKOV3. Non-loaded nanoparticles (NP-empty), paclitaxel-loaded nanoparticles (NP-Taxel) and paclitaxel alone at the stated concentrations were added to the cancer cell cultures for 48 h, and cytotoxicity was measured by MTS. The treatments were 48 h with NP-Taxel or paclitaxel alone. \* $p < 0.05$  compared to the control; # $p < 0.05$  compared to the NP empty vector; ANOVA, post-test Bonferroni.

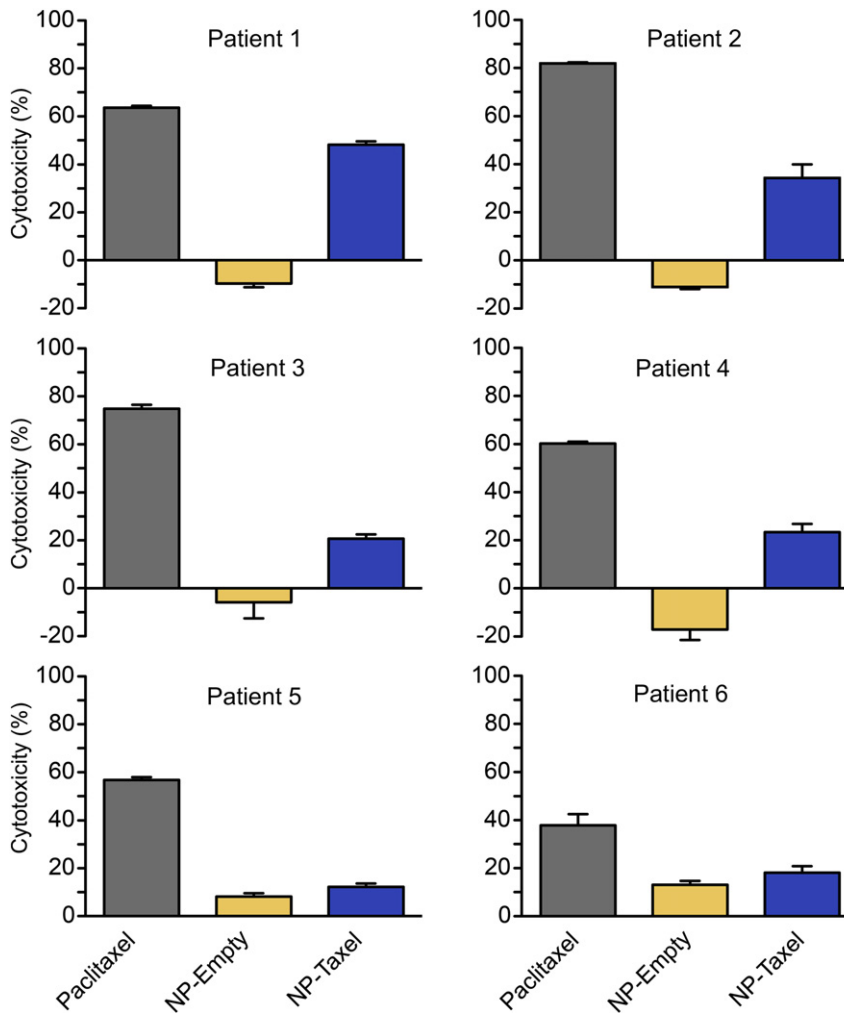


**Fig. 9.** NP-Taxel induces cell death in primary cultured human ovarian cancer cells. The cancer cells were obtained with informed consent from either the primary tumor or peritoneal fluid (ascitis) of patients with stage IIIc papillary serous ovarian cancer. The percentage of cytotoxicity was measured by MTS after incubation for 48 h with 5 μM paclitaxel-loaded nanoparticles (NP-Taxel), non-loaded nanoparticles (NP-empty) or paclitaxel alone.

potentially protective effects of PHBV, any future PHBV nanoparticle will come loaded with a chemotherapeutic drug and will therefore make cell death more likely to occur.

While these PHBV nanoparticles displayed minimal drug release in solution and minor cytotoxicity toward primary cultured ovarian cancer cells, there are other ways in which these nanoparticles could be improved for future clinical application. For instance, an increase in the loading of the nanoparticles that would give an average release of a minimum of 1–10  $\mu\text{M}$  paclitaxel should result in cancer cell toxicity that is similar to that of paclitaxel alone and will hopefully confer fewer side effects. To this end, further investigation is required to optimize the ratios of PHBV and paclitaxel in the starting emulsion and to determine the saturation point of paclitaxel loading. A better understanding of the optimal timing of drug release in terms of cytotoxicity may allow for the precise selection of the liberation rate, which could be altered by using a PHBV with a lower molecular weight or a PHBV with a higher composition of valerate. Further improvements are necessary to expand upon the passive targeting of nanoparticles by adding an active uptake component to this preparation method. The surface incorporation of folic acid, which is preferentially taken up by cancer cells, or the addition of aptamer bioconjugates may add greater specificity and intracellular drug accumulation.

#### 4. Conclusion

Here, we describe an integrated study that includes the molecular simulation, physicochemical characterization and biological evaluation of a paclitaxel-loaded PHBV nanoparticles. Molecular simulation displayed a high affinity of paclitaxel for the water–polymer interface and porous nanoparticle structure. The particles size range 228–264 nm makes them appropriate for passive targeting by EPR effect, and their negative charge ( $-6$  to  $-8.9$  mV), suitable for the biological environment. The analysis of NP-Taxel by low voltage electron microscopy and FTIR during in vitro degradation process revealed the presence of branched structures on the surface of particles, and the generation of new chemical bonds suggesting a temporal crystalline phase in the first 3 days. Finally, the NP-Taxel exhibited a low in vitro rate of release, intracellular uptake, and a high cytotoxic capacity in cell lines, and in primary cultures of stage IIIc serous ovarian cancer cells isolated from six patients. The promising results and the low cost of production, supports PHBVs as strong candidates in the development of novel drug-loaded nanoparticles for large-scale production by the pharmaceutical industry.

#### Author contribution

C.V. and L.A.V. planned the experiments. C.V. and F.M. formulated the nanoparticles. P.S. and N.H. performed the physicochemical characterization. F.G.N. and J.C. developed the dynamic molecular modeling. D.A. and H.M. performed the electron microscopy analysis. P.G., S.K., M.A.C., C.A. and E.B. obtained the patient samples for the primary cultures. M.L.B. and G.I.O. studied the antitumor activity cancer cells. C.V., G.I.O., F.G.N. and L.A.V. analyzed the data and wrote the paper.

#### Funding

The authors declare no competing financial interests.

#### Acknowledgments

We thank the medical institutions, the medical staff and the patients for their generous participation and donation of primary

tissue. This research was supported by the: Centro para el Desarrollo de la Nanociencia y Nanotecnología (CEDENNA); FB0807 (C.V., F.M., L.A.V.); and the Biomedical Research Consortium of Chile; CTU06 (G.I.O.). Finally, we acknowledge Fondo Nacional de Desarrollo Científico y Tecnológico Gobierno de Chile (FONDECYT) 1120712 (L.A.V.), 1080163 (M.A.C.), 1100870 (G.I.O.), and 3120003 (M.L.B.).

#### Appendix A. Supplementary data

Supplementary data related to this article can be found at <http://dx.doi.org/10.1016/j.biomaterials.2013.02.034>.

#### References

- [1] Jemal A, Siegel R, Xu J, Ward E. Cancer statistics. *CA Cancer J Clin* 2010; 2010(60):277–300.
- [2] Bast Jr RC, Hennessy B, Mills GB. The biology of ovarian cancer: new opportunities for translation. *Nat Rev Cancer* 2009;9:415–28.
- [3] Vaughan S, Coward JI, Bast Jr RC, Berchuck A, Berek JS, Brenton JD, et al. Rethinking ovarian cancer: recommendations for improving outcomes. *Nat Rev Cancer* 2011;11:719–25.
- [4] Arias JL. Drug targeting strategies in cancer treatment: an overview. *Mini Rev Med Chem* 2011;11:1–17.
- [5] Wang AZ, Langer R, Farokhzad OC. Nanoparticle delivery of cancer drugs. *Annu Rev Med* 2012;63:185–98.
- [6] Wagner V, Dullaart A, Bock AK, Zweck A. The emerging nanomedicine landscape. *Nat Biotechnol* 2006;24:1211–7.
- [7] Dhar S, Kolishetti N, Lippard SJ, Farokhzad OC. Targeted delivery of a cisplatin prodrug for safer and more effective prostate cancer therapy in vivo. *Proc Natl Acad Sci USA* 2011;108:1850–5.
- [8] Shi J, Xiao Z, Votruba AR, Vilos C, Farokhzad OC. Differentially charged hollow core/shell lipid–polymer–lipid hybrid nanoparticles for small interfering RNA delivery. *Angew Chem Int Ed Engl* 2011;50:7027–31.
- [9] Wohlfart S, Gelperina S, Kreuter J. Transport of drugs across the blood–brain barrier by nanoparticles. *J Control Release* 2012;161:264–73.
- [10] Xie J, Liu G, Eden HS, Ai H, Chen X. Surface-engineered magnetic nanoparticle platforms for cancer imaging and therapy. *Acc Chem Res* 2011;44:883–92.
- [11] Kumari A, Yadav SK, Yadav SC. Biodegradable polymeric nanoparticles based drug delivery systems. *Colloids Surf B Biointerfaces* 2010;75:1–18.
- [12] Cragg GM, Newman DJ. A tale of two tumor targets: topoisomerase I and tubulin. The Wall and Wani contribution to cancer chemotherapy. *J Nat Prod* 2004;67:232–44.
- [13] Acharya S, Sahoo SK. PLGA nanoparticles containing various anticancer agents and tumour delivery by EPR effect. *Adv Drug Deliv Rev* 2011;63:170–83.
- [14] Slater S, Mitsky TA, Houmiel KL, Hao M, Reiser SE, Taylor NB, et al. Metabolic engineering of Arabidopsis and Brassica for poly(3-hydroxybutyrate-co-3-hydroxyvalerate) copolymer production. *Nat Biotechnol* 1999;17:1011–6.
- [15] Kuppam P, Vasanthan KS, Sundaramurthi D, Krishnan UM, Sethuraman S. Development of poly(3-hydroxybutyrate-co-3-hydroxyvalerate) fibers for skin tissue engineering: effects of topography, mechanical, and chemical stimuli. *Biomacromolecules* 2011;12:3156–65.
- [16] Sendil D, Gursel I, Wise DL, Hasirci V. Antibiotic release from biodegradable PHBV microparticles. *J Control Release* 1999;59:207–17.
- [17] Vilos C, Velasquez LA. Therapeutic strategies based on polymeric microparticles. *J Biomed Biotechnol* 2012;2012:672760.
- [18] Vilos C, Constandil L, Herrera N, Solar P, Escobar-Fica J, Velasquez LA. Cef-tiofur-loaded PHBV microparticles: a potential formulation for a long-acting antibiotic to treat animal infections. *Electron J Biotechnol* 2012;15:1–13.
- [19] Sahana B, Santra K, Basu S, Mukherjee B. Development of biodegradable polymer based tamoxifen citrate loaded nanoparticles and effect of some manufacturing process parameters on them: a physicochemical and in-vitro evaluation. *Int J Nanomedicine* 2010;5:621–30.
- [20] Mao S, Xu J, Cai C, Germershaus O, Schaper A, Kissel T. Effect of WOW process parameters on morphology and burst release of FITC-dextran loaded PLGA microspheres. *Int J Pharm* 2007;334:137–48.
- [21] Zhang SQ, Chen GH. Determination of paclitaxel in human plasma by UPLC-MS-MS. *J Chromatogr Sci* 2008;46:220–4.
- [22] Vanommeslaeghe K, Hatcher E, Acharya C, Kundu S, Zhong S, Shim J, et al. CHARMM general force field: a force field for drug-like molecules compatible with the CHARMM all-atom additive biological force fields. *J Comput Chem* 2010;31:671–90.
- [23] Phillips JC, Braun R, Wang W, Gumbart J, Tajkhorshid E, Villa E, et al. Scalable molecular dynamics with NAMD. *J Comput Chem* 2005;26:1781–802.
- [24] Wells DB, Bhattacharya S, Carr R, Maffeo C, Ho A, Comer J, et al. Optimization of the molecular dynamics method for simulations of DNA and ion transport through biological nanopores. *Methods Mol Biol* 2012;870:165–86.
- [25] Darve E, Rodriguez-Gomez D, Pohorille A. Adaptive biasing force method for scalar and vector free energy calculations. *J Chem Phys* 2008;128:144120.

- [26] Henin J, Fiorin G, Chipot C, Klein M. Exploring multidimensional free energy landscapes using time-dependent biases on collective variables. *J Chem Theory Comput* 2009;6:35–47.
- [27] Marrink SJ, Risselada HJ, Yefimov S, Tieleman DP, de Vries AH. The MARTINI force field: coarse grained model for biomolecular simulations. *J Phys Chem B* 2007;111:7812–24.
- [28] Hess B, Kutzner C, Van Der Spoel D, Lindahl E. GROMACS 4: algorithms for highly efficient, load-balanced, and scalable molecular simulation. *J Chem Theory Comput* 2008;4:435–47.
- [29] Bussi G, Donadio D, Parrinello M. Canonical sampling through velocity rescaling. *J Chem Phys* 2007;126:014101.
- [30] Nishida M. The Ishikawa cells from birth to the present. *Hum Cell* 2002;15:104–17.
- [31] Hill BT, Whelan RD, Gibby EM, Sheer D, Hosking LK, Shellard SA, et al. Establishment and characterisation of three new human ovarian carcinoma cell lines and initial evaluation of their potential in experimental chemotherapy studies. *Int J Cancer* 1987;39:219–25.
- [32] Kato S, Sadarangani A, Lange S, Delpiano A, Vargas M, Brañes J, et al. 2-methoxyestradiol mediates apoptosis through caspase-dependent and independent mechanisms in ovarian cancer cells but not in normal counterparts. *Reprod Sci* 2008;15:878–94.
- [33] Sadarangani A, Kato S, Espinoza N, Lange S, Lladós C, Espinosa M, et al. TRAIL mediates apoptosis in cancerous but not normal primary cultured cells of the human reproductive tract. *Apoptosis* 2007;12:73–85.
- [34] Peer D, Karp JM, Hong S, Farokhzad OC, Margalit R, Langer R. Nanocarriers as an emerging platform for cancer therapy. *Nat Nanotechnol* 2007;2:751–60.
- [35] Nel AE, Madler L, Velegol D, Xia T, Hoek EM, Somasundaran P, et al. Understanding biophysicochemical interactions at the nano-bio interface. *Nat Mater* 2009;8:543–57.
- [36] Loverde SM, Klein ML, Discher DE. Nanoparticle shape improves delivery: rational coarse grain molecular dynamics (rCG-MD) of taxol in worm-like PEG-PCL Micelles. *Adv Mater* 2012;24:3823–30.
- [37] Li H, Chang J. Preparation, characterization and in vitro release of gentamicin from PHBV/wollastonite composite microspheres. *J Control Release* 2005;107:463–73.
- [38] Hunz M, Jetter A, Warm M, Pantke E, Tuscher M, Hempel G, et al. Plasma and tissue pharmacokinetics of epirubicin and Paclitaxel in patients receiving neoadjuvant chemotherapy for locally advanced primary breast cancer. *Clin Pharmacol Ther* 2007;81:659–68.
- [39] Xiao XQ, Zhao Y, Chen GQ. The effect of 3-hydroxybutyrate and its derivatives on the growth of glial cells. *Biomaterials* 2007;28:3608–16.
- [40] Cheng B, Yang X, Chen C, Cheng D, Xu X, Zhang X. D-beta-hydroxybutyrate prevents MPP+ induced neurotoxicity in PC12 cells. *Neurochem Res* 2010;35:444–51.
- [41] Hu ZG, Wang HD, Jin W, Yin HX. Ketogenic diet reduces cytochrome c release and cellular apoptosis following traumatic brain injury in juvenile rats. *Ann Clin Lab Sci* 2009;39:76–83.